Microfluidics and Nanofluidics manuscript No.
(will be inserted by the editor)

Breakup length of AC electrified jets in a microfluidic flow-focusing junction

Elena Castro-Hernández · Pablo García-Sánchez · Say Hwa Tan · Alfonso M. Gañán-Calvo · Jean-Christophe Baret · Antonio Ramos

Received: date / Accepted: date

Abstract Electroactuation of liquid-liquid interfaces offers promising methods to actively modulate droplet formation in droplet-based microfluidic systems. Here, flow-focusing junctions are coupled to electrodes to control droplet production in the well-known jetting regime. In this regime, a convective instability develops leading to droplet formation at the end of a thin and uniform, long liquid finger. We show that in AC electric fields the jet length is a function of both the magnitude of the applied voltage and the electrical parameters such as the frequency of the AC field and the conductivity of the dispersed phase. We explain that dependency using a simple transmission line model along the liquid jet. An optimum frequency to maximize the liquid ligament length is experimentally observed. Such length simply cannot be obtained by other means under the same operating conditions, in the absence of the AC signal. At low frequency, we reach a transition from a well-behaved, uniform jet brought about near the optimum frequency to highly unstable liquid structures in which axisymmetry is lost rather abruptly.

Keywords AC electric field · flow focusing · microfluidics · jet

Elena Castro-Hernández · Alfonso M. Gañán-Calvo
Área de Mecánica de Fluidos, Departamento de Ingeniería Aeroespacial y Mecánica de Fluidos, Universidad de Sevilla, Avenida de los Descubrimientos s/n 41092, Sevilla, Spain.
E-mail: elenacastro@us.es

Pablo García-Sánchez · Antonio Ramos
Departamento de Electrónica y Electromagnetismo, Facultad de Física, Universidad de Sevilla, Avenida de Reina Mercedes s/n, 41012 Sevilla, Spain.
E-mail: ramos@us.es

Say Hwa Tan
Queensland Micro- and Nanotechnology Centre, Griffith University, Brisbane QLD 4111, Australia and Max-Planck Institute for Dynamics and Self-Organization, Droplets, Membranes and Interfaces, Am Fassberg 17, DE-37077 Goettingen.

Jean-Christophe Baret
CNRS, Univ. Bordeaux, CRPP, UPR 8641, Soft Micro Systems, 115 Avenue Schweitzer, 33600 Pessac, France and Max-Planck Institute for Dynamics and Self-Organization, Droplets, Membranes and Interfaces, Am Fassberg 17, DE-37077 Goettingen.

1 Introduction

Droplet-based microfluidics provides new means to miniaturize and automatize biochemical reactions for ultra-high throughput screening applications (Miller et al., 2006; Huebner et al., 2008; Seemann et al., 2012; Guo et al., 2012). The controlled production and manipulation of monodisperse droplets of well-defined volume is of key interest to many applications ranging from diagnostics in emulsion PCR (Pekin et al., 2011) and cell screening (Agresti et al., 2010; Debs et al., 2012) to drug screening (Miller et al., 2012). At the core of the technology lies droplet production. Several systems are compatible with ultra-high throughput droplet production. T-junction (Thorsen et al., 2001), flow-focusing (Anna and Mayer, 2006), co-flow (Cramer et al., 2004) and step emulsification (Dangla et al., 2013) geometries provide a reliable and controllable environment for monodispersed droplet generation. However, the unceasing needs for enhanced functionalities and control has driven the development of alternative methods to actively control droplet generation. These methods are based on external perturbation, through thermal (Tan et al., 2008), magnetic (Nguyen et al., 2006; Tan and Nguyen,

2011), acoustic (Schmid and Franke, 2013), pneumatic (Abate et al., 2009) or electrical (Kim et al., 2007; Malloggi et al., 2008) modulation of the liquid properties. To date, electrical control has proven to be the most robust, reliable and rapid mode for microdroplets actuation in microfluidic devices. Sorting droplets with electric field is achieved at rates up to 30 kHz in microfluidics (Sciambi and Abate, 2014) and is the central ingredient in commercial Fluorescence-Activated cell sorters which function at similar throughputs (Ashcroft and Lopez, 2000). Electric fields offer promissing routes to control droplet production. Using the combined effects of focused forces of hydrodynamic and electrical origin in a direct current (DC) was early proposed by Gañán-Calvo *et al.* (Gañán-Calvo, 2002; Gañán-Calvo, 2007; Gañán-Calvo et al., 2006; Gañán-Calvo and López-Herrera, 2002) followed by Kim et al. (2007). The use of an alternating current (AC) by Malloggi et al. (2008) and Tan et al. (2014b) has provided further avenues for exploration: well-defined microdroplets of desired sizes can be manipulated and formed repeatedly in the order of milli-seconds or faster, in operating regimes where the absence of electric fields or the use of DC ones does not allow that control. Indeed, we have demonstrated a new method of droplet generation in microfluidic devices using an AC voltage mediated electric field (Tan et al., 2014b), where microdroplet production is electrically controlled in the dripping or jetting regime (Cubaud and Mason, 2008) depending on the applied voltage, electrode configuration and physical properties of the fluids. This method of control has also been extended to demonstrate reliable droplet generation and manipulation via a musical interpretation of droplet based microfluidics (Tan et al., 2014a).

In both DC (Gañán-Calvo et al., 2006; Kim et al., 2007) or AC (Tan et al., 2014b) electroflow-focusing, three different regimes are identified : Dripping, axisymmetric jetting and *unstable* regime. The dripping regime is characterized by the generation of droplets close to the orifice, within a distance equal to one orifice diameter. In contrast, when jetting occurs, the droplets are produced at the end of a jet that extends at least three orifice diameters (Gañán-Calvo, 1998; Anna et al., 2003). In an AC field the unstable regime is observed at low values of the frequency field. Here the jet breaks in a random manner producing polydisperse droplets and approaching alternatively both PDMS walls without any characteristic periodicity. The transitions between these regimes are not fully understood although a qualitative behavior has been identified for the relevant parameters of this problem. If the high-voltage is applied to the downstream pair of electrodes while the others are grounded, the only transition that is observed is from the jetting to the unstable regimes (Tan et al., 2014b). This is the configuration that will be study in this paper.

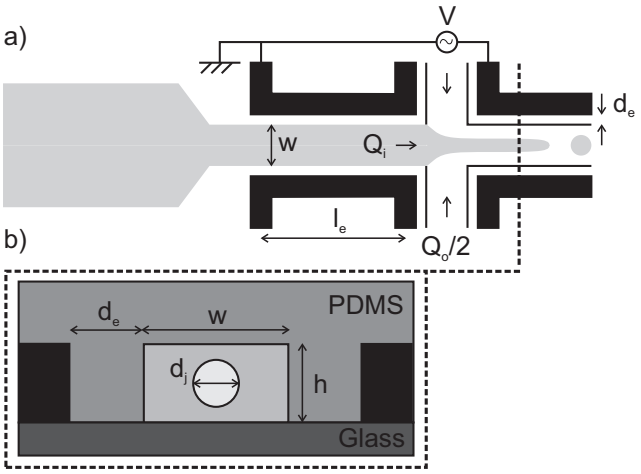

Fig. 1 a) Sketch of a microfluidic flow-focusing junction under an AC electric field. The electrodes are in black and the aqueous phase in grey. b) Cross section of the device at the level of the downstream electrodes.

In this work, we investigate the role of electric field in the jetting regime. The effect of viscosities of the continuous phase fluids, applied frequencies and voltages are studied with a focus on the breakup length of the jet. A minimal model is also proposed to describe the length of the jet in the corresponding electrical parameters. In addition, the transition between the axisymmetric jet and the unstable droplet production has been observed at low frequency and experimentally characterized.

2 Experimental setup

Soft lithography techniques are used to manufacture a microfluidic flow-focusing junction by replica molding in polydimethylsiloxane (PDMS, Dow Corning, relative permittivity $\varepsilon_{r,\mathrm{PDMS}} = 2.5$). Microfluidic channels in the device are $100\,\mu$m wide and $35\,\mu$m tall, w and h respectively in figure 1. Two pairs of electrodes are patterned around the junction as microfluidic channels and produced using the microsolidics technique (Siegel et al., 2006) as described in Tan et al. (2014b). The spacing between the electrodes and the fluidic channel is $d_e = 35\,\mu$m over a length $l_e = 2.2\,$mm (figure 1). The PDMS device is plasma bonded to the non-conductive side of an Indium Tin Oxide glass (ITO, thickness 1 mm, $\varepsilon_{r,\mathrm{glass}} = 7.5$). The conductive side of the ITO glass is used as a counter electrode.

Water-in-oil (W/O) droplets are formed by focusing an aqueous stream (dispersed phase) with two side oil streams (continuous phase). The inner and outer volumetric flow rates, Q_i and Q_o, are controlled using a syringe pump (Model 33, Harvard Apparatus). The dispersed phase is an aqueous solution of NaCl in Milli-Q water with a viscosity $\eta_i = 1\,\mathrm{cP}$ and an electrical conductivity varying between $\kappa = 3 \times 10^{-4}\,\mathrm{S/m}$ and $\kappa = 3 \times 10^{-3}\,\mathrm{S/m}$. The continuous phase is mineral oil (RTM14, Sigma Aldrich) with a viscosity between $\eta_o = 1\,\mathrm{cP}$ and $\eta_o = 100\,\mathrm{cP}$. The relative permittivity of mineral oil is $\varepsilon_{r,o} = 2.1$ and its electrical conductivity is negligible ($\kappa_o < 10^{-10}\,\mathrm{S/m}$), *i.e.* it is considered here as a perfect insulator. A 5 % (w/w) of a non-ionic surfactant (Span 80, Sigma Aldrich) is added to the continuous phase lowering the equilibrium surface tension of the liquid-liquid interface from $\sigma = 40\,\mathrm{mN/m}$ to $\sigma = 5\,\mathrm{mN/m}$, this value being independent of the NaCl concentration.

In principle, with the configuration of the three electrodes (upstream pairs, downstream pairs and ITO) and the two possible connections generates 2^3 possible connnections. However, removing the trivial cases where all electrodes have the same voltage and making use of symmetries, only three different electrical configurations remain (Tan et al., 2014b). Here, we focus on the single case where the high-voltage is applied to the downstream pair of electrodes, while the others were grounded. This configuration guarantees that the incoming liquid has zero potential (Tan et al., 2014b). As a consequence, there is an applied AC potential difference between the inner liquid emerging from the upstream electrodes and the downstream electrodes. A sinusoidal voltage with frequencies ranging from $f = 1\,\mathrm{kHz}$ to $f = 50\,\mathrm{kHz}$ (TGA1244, TTi) is amplified from $V = 0\,\mathrm{V}$ to $V = 1000\,\mathrm{V}$ (PZD700A, Trek). In the following discussion, all voltages are peak to peak. The setup is placed on an inverted microscope (Eclipse Ti-U, Nikon) connected to a high-speed camera (Phantom v7.3) with a resolution of $800 \times 256\,\mathrm{px}^2$ when operated at an acquisition rate of 10^4 fps. The jet diameter, d_j, and jet length, l_j, of at least 100 images are measured via image processing (Matlab, Mathworks and ImageJ).

3 Experimental results

We perform series of experiments varying the outer viscosities ($\eta_o = 1$, 10 and 100 cP), the inner conductivities ($\kappa = 3 \times 10^{-4}$, 1×10^{-3} and $3 \times 10^{-3}\,\mathrm{S/m}$), the frequency of the AC field ($f = 0 - 50\,\mathrm{kHz}$), the inner to outer flow rate ratio ($Q_i/Q_o = 0.125$, 0.25 and 0.5) and the voltage ($V = 0$, 250, 750 and 1000 V).

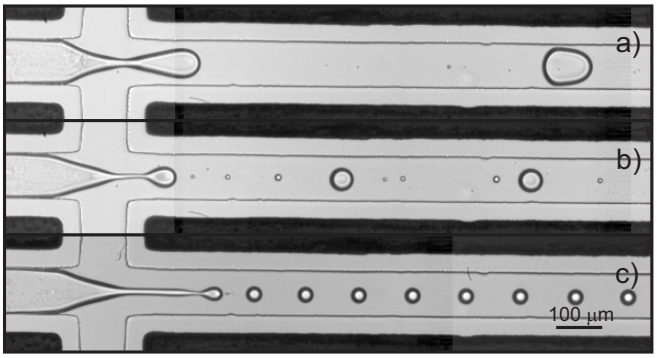

Fig. 2 Series of images showing the effect of increasing the voltage on the jet length for $Q_i = 50\,\mu\mathrm{l/h}$, $Q_o = 400\,\mu\mathrm{l/h}$, $\eta_o = 10\,\mathrm{cP}$, $\kappa = 1 \times 10^{-3}\,\mathrm{S/m}$ and $f = 40\,\mathrm{kHz}$: a)$V = 250\,\mathrm{V}$; b)$V = 750\,\mathrm{V}$; c)$V = 1000\,\mathrm{V}$.

Figure 2 shows a series of images for a given flow rate ratio, water conductivity and an outer fluid viscosity $\eta_o = 10\,\mathrm{cP}$.
The frequency is fixed at 40 kHz and, according to previous results (Tan et al., 2014b), a dripping to jetting transition is reached when the voltage amplitude increases. A further increase in voltage results in longer jets and, for $\eta_o = 10\,\mathrm{cP}$, a jet of $200\,\mu\mathrm{m}$ in length is obtained when the maximum voltage supplied by the amplifier is applied (1000 V). The same qualitative behavior is found for the two other viscosities with the remarkable observation that, for $\eta_o = 100\,\mathrm{cP}$, we observe slender jets and, in some cases, longer than the channel length (3 mm). An analogous phenomenon has been reported by some authors without the presence of an electric field (Gañán-Calvo et al., 2007; Gañán-Calvo, 2008; Utada et al., 2008; Cubaud and Mason, 2008; Cordero et al., 2011; Castro-Hernández et al., 2012), and explained via more or less elaborated spatiotemporal stability analyses (Guillot et al., 2007, 2008; Gañán-Calvo, 2008). A remarkable result found was that an unconditionally stable jetting can be obtained independently of the jet diameter (theoretically, down to the continuum limit) for asymptotically low Reynolds numbers when a properly defined Capillary number $Ca^* = (\eta_i \eta_o)^{1/2} U_i/\sigma$ is above a certain critical threshold, being U_i the velocity of the continuous phase surrounding the jet (Gañán-Calvo, 2008) (strictly speaking, U_i should be the velocity at the jet surface). In that case, even with liquids begetting very small inner capillary number $Ca_i = \eta_i U_i/\sigma$ (e.g. liquid metals like mercury), one may obtain jets and droplets down to nanometric size as long as Ca^* is above the limit threshold, which so far has been experimentally confirmed at different instances (Gañán-Calvo et al., 2007; Gopalan and Katz, 2010). Here, we show that the simple use of an AC voltage dramatically elongates the jets

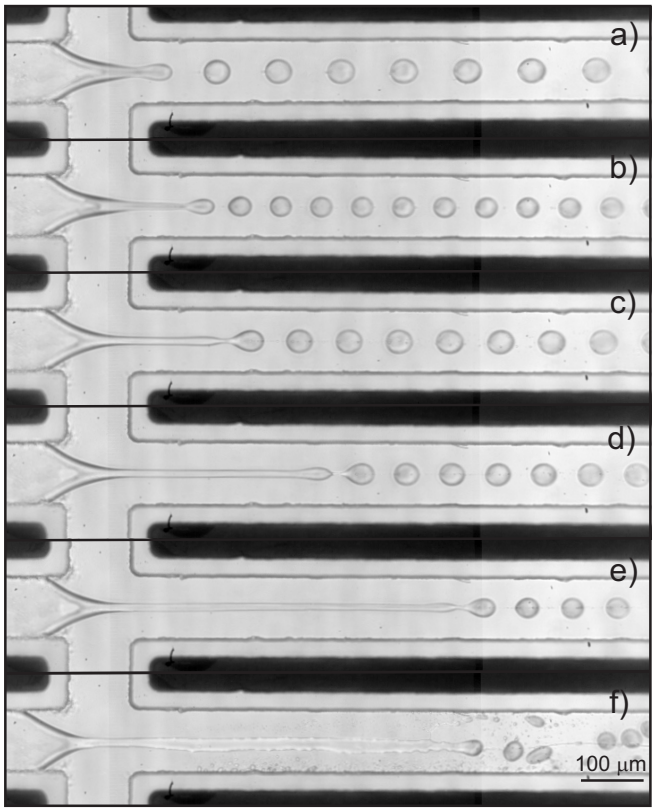

Fig. 3 Series of images showing the effect of decreasing the frequency field on the jet length for $Q_i = 50\,\mu$l/h, $Q_o = 400\,\mu$l/h, $\eta_o = 100\,$cP, $\kappa = 3 \times 10^{-4}\,$S/m and $V = 1000\,$V: a)$V = 0\,$V; b)$f = 50\,$kHz; c)$f = 30\,$kHz; d)$f = 5\,$kHz; e)$f = 3\,$kHz; f)$f = 1\,$kHz.

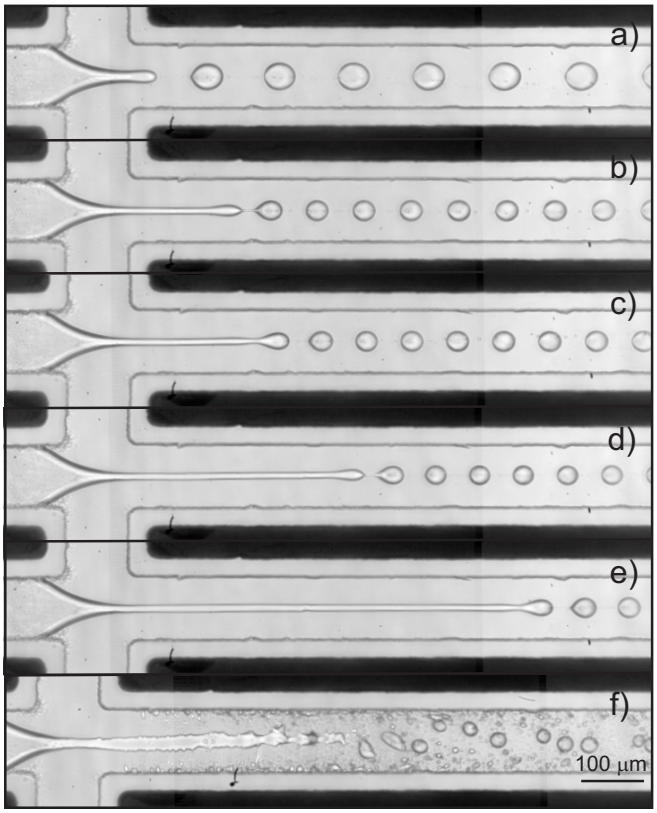

Fig. 4 Series of images showing the effect of decreasing the frequency field on the jet length for $Q_i = 50\,\mu$l/h, $Q_o = 400\,\mu$l/h, $\eta_o = 100\,$cP, $\kappa = 1 \times 10^{-3}\,$S/m and $V = 1000\,$V: a)$V = 0\,$V; b)$f = 50\,$kHz; c)$f = 30\,$kHz; d)$f = 10\,$kHz; e)$f = 5\,$kHz; f)$f = 1\,$kHz.

and might provide a technological advantage for manufacturing processes where structures with large aspect ratios are required.

Ancient experience shows that very long jets are easily obtained when a high viscosity liquid is stretched by sustained forces of many different origins (Eggers and Villermaux, 2008). However, as the capillary number of the developing jet decreases, so does its length in a more or less drastic fashion, depending on the nature of the surrounding environment. The available methods to get thin, very long jets of low viscosity liquids like water virtually reduce to zero when the diameter ranges sought for decrease down to the micrometric range or below, unless a sufficiently viscous environment is used. In this case, experimentally confirmed results from spatiotemporal stability analyses (Gañán-Calvo et al., 2007; Gañán-Calvo, 2008) predict convective instability (jetting) down to the molecular length scale if the geometrically averaged capillary number Ca^* is above 0.2 (approx.), for $\eta_o/\eta_i > 0.1$. Thus, for the sake of efficiency, we fix the velocity of the surrounding environment, keeping the outer flow rate as $Q_o = 400\,\mu$l/h in this study. Assuming that the radial diffusion of momentum is rapid (low Reynolds inner liquid flow), one can reasonably expect that the size and average velocity of the liquid jet will immediately adjust to the one imposed by the environment and mass conservation constrains. Given the fixed viscosity of the liquid jet, $\eta_i = 1\,$cP, and the geometrical constrains of our system, relatively straightforward numerical resolution of the resulting unperturbed creeping flow (e.g. see for details Herrada et al. (2008)) provides $Ca^* = 0.014$, 0.05, and 0.16 for $\eta_o = 1$, 10 and 100 cP, respectively. Here, we assume that the jet occupies the central axis of the channel, where the outer velocity is slightly over double of the average one $U_o = Q_o/wh$ for low Reynolds flow. Spatiotemporal stability predicts (Herrada et al., 2008) stable jetting (convectively unstable flow) for the case $Ca^* = 0.16$ only. Thus, in order to study these long jets, we focused in experiments with an outer fluid viscosity $\eta_o = 100\,$cP. Figures 3, 4 and 5 show three series of images corresponding to $\eta_o = 100\,$cP and three different conductivities of the dispersed phase. The flow rate ratio ($Q_i = 50\,\mu$l/h and $Q_o = 400\,\mu$l/h) corresponds to a situation in which jetting occurs even in the absence of electric field although with smaller jet lengths (Figures

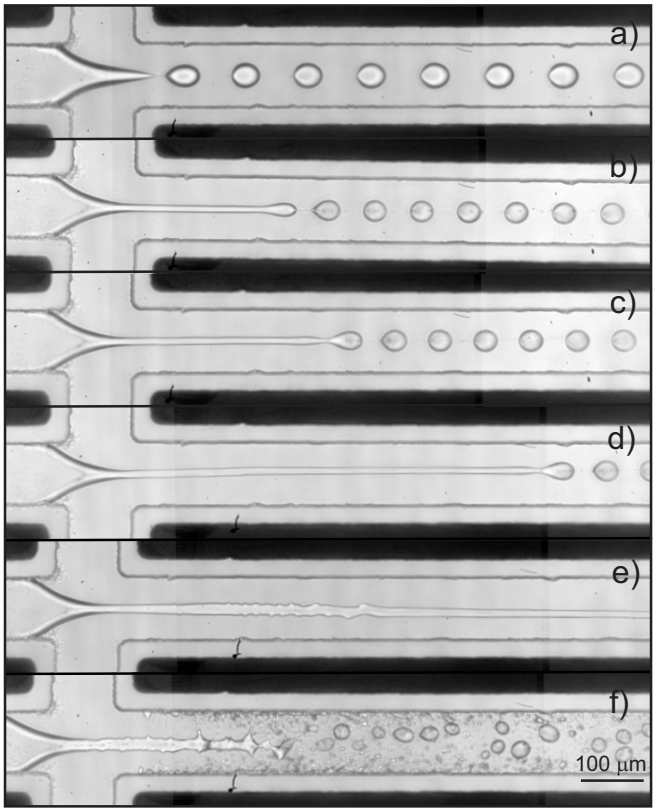

Fig. 5 Series of images showing the effect of decreasing the frequency field on the jet length for $Q_i = 50\,\mu$l/h, $Q_o = 400\,\mu$l/h, $\eta_o = 100\,$cP, $\kappa = 3 \times 10^{-3}\,$S/m and $V = 1000\,$V: a)$V = 0\,$V; b)$f = 50\,$kHz; c)$f = 30\,$kHz; d)$f = 10\,$kHz; e)$f = 3\,$kHz; f)$f = 1\,$kHz.

3a, 4a, 5a). AC signals of amplitude $V = 1000\,$V were applied and, for all conductivities, longer jets are found as the frequency of the signal was reduced (sequence from b to e in the figures). For a fixed frequency longer jets are obtained for liquids with higher conductivities. Figures 3f, 4f and 5f show that the *unstable* regime is observed for frequencies low enough ($f \leq f_{\text{mess}} \simeq 3\,$kHz). Apparently, this transition frequency to the unstable regime does not depend much on water conductivity for $\eta_o = 100\,$cP. This is different from the observations reported by Tan et al. (2014b), where a transition from jetting to unstable drop production was found for a frequency which linearly increases with water conductivity for $\eta_o = 30\,$cP. In the present experiments, the unstable regime might be a different phenomenon since a long jet is formed and remains when the instability takes place. From this moment the jet wets the wall and produces liquid filaments that eventually break into droplets of different sizes. A possible reason for the instability is that the jet at the center of the channel is a situation potentially unstable. The jet is attracted to both electrodes, due to the voltage difference with respect to them, and any nonsymmetrical perturbation can be amplified if the electric field is high enough. The appearance of this instability at a certain frequency and below lacks of a theoretical explanation.

Figure 6 shows the jet length, l_j, as a function of signal frequency for the three water conductivities. The jet length is measured from the begining of the downstream electrodes. If we plot the dimensional quantities l_j versus f/κ, all data points collapse onto a single master curve as depicted in the inset of figure 6. The figure also shows the best-fit curve with power $-1/2$. This key clue provided by the experimental data will be confirmed by theoretical analysis (see section 4).

We have also tested smaller values of the outer flow rate: $Q_o = 100\,\mu$l/h and $Q_o = 50\,\mu$l/h. When the AC electric field is applied smaller values of l_j are obtained, as expected, and the same trends are found. Interestingly, f_{mess} increases from $f_{\text{mess}} \simeq 3\,$kHz to $f_{\text{mess}} \simeq 9\,$kHz when Q_o is decreased from $Q_o = 400\,\mu$l/h to $Q_o = 50\,\mu$l/h.
Besides, we have performed experiments for outer viscosities $\eta_o = 1\,$cP and $\eta_o = 10\,$cP. In these cases in absence of an electric field the dripping regime takes place, as predicted by the spatiotemporal stability analysis (Herrada et al., 2008). With these values of the viscosities, shorter jets are obtained unless very high values of the outer velocities are used. As a consequence, these experiments were not adequate to our study of long jets. Nevertheless, a relevant behavior was noted: if the rest of the parameters are fixed (Q_i, Q_o, κ, V and f) when η_o is decreased f_{mess} increases. Particularly, for the case $\eta_o = 1\,$cP the unstable regime was always present. However, the spatiotemporal stability analysis of our system in the presence of electric fields (DC or AC) and a detailed account of the parametrical dependence of those features is out of the scope of present work and the object of a subsequent one.

4 Discussion

Let us summarize the main dimensionless numbers involved in this problem. Once the viscosity ratio and flow rate ratio are fixed, it can be seen from the table 1 that the inner and outer Reynolds numbers are small, which tell us that inertial effects are negligible as it is usual in these types of geometries. Here $U_i = 4Q_i/\pi d_j^2$ is the average velocity of the dispersed phase. The electrical Bond number B_e is defined as the time-averaged electrical pressure on the interface $\varepsilon_o E_{rms}^2/2$ divided by the capillary pressure σ/ℓ, where ℓ is a typical radius of curvature. A characteristic value

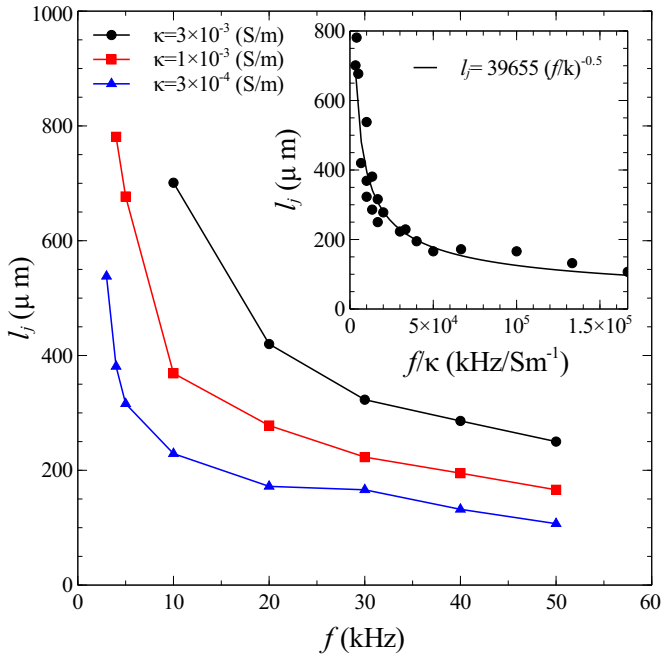

Fig. 6 Jet length versus frequency field for different values of the conductivity for $Q_i = 50\,\mu$l/h, $Q_o = 400\,\mu$l/h, $\eta_o = 100\,$cP and $V = 1000\,$V. The inset shows l_j versus f/κ.

of the electrical Bond number for the cone-jet transition is $B_{\mathrm{e,cone}} \sim 0.5$, taking as typical cone radius of curvature $\ell = 20\,\mu$m and a characteristic electric field on the cone surface $E_{rms} = 3.5\times10^6$ V/m. Since the radius of the jet is measured experimentally and almost constant $d_j/2 = 6.5\,\mu$m and the electric field on the surface of the jet is $E_{rms} = 2.3\times10^7$ V/m (computed numerically using finite elements), the electrical Bond number for the jet becomes $B_{\mathrm{e,jet}} \sim 6$. This indicates that in the cone-to-jet transition B_e changes by an order of magnitude. While the inner and outer capillary numbers are below unity, the electrical Bond number of the jet is much greater, reassuring the fact that the electric forces are responsible for the formation of such long jets.

The experiments show that there is a long jet when there is both a high applied voltage and sufficient low frequency. When either the applied voltage is zero or the frequency is high, there is a very short jet that breaks into drops rapidly. Based upon these experimental facts, we can think that the jet breaks into drops when the electric field amplitude around the jet tip is below a certain value. Let us study the voltage difference between the jet and the channel electrodes as a function of distance along the jet. This voltage difference is maximum at the channel entrance and decreases for increasing distance inside the channel. Eventually, this voltage difference would be zero when the jet voltage adapts to the surrounding voltage and we can think that near this point is when the jet breaks into drops. We are going to use concepts of transmission line, or distributed element, theory (Ramo et al., 2008) applied to a very long jet, ideally infinitely long. This transmission line model is valid when there is translational symmetry and the characteristic length along the line is much greater than the characteristic length in transverse direction. Let V_0 be the potential difference between the jet and the electrodes at the channel entrance ($z = 0$). The potential drop in the axial direction along a resistive jet is

$$V(z) - V(z+dz) = \frac{dz}{\kappa\pi a^2} I(z) \Rightarrow -\frac{\partial V}{\partial z} = \frac{I}{\kappa\pi a^2} \qquad (1)$$

where $I(z)$ is the current intensity carried by the jet at z, κ is the liquid conductivity and $a = d_j/2$ is the jet radius. From charge conservation, the current intensity at z is equal to the current at $z+dz$ plus the displacement current leaving the jet interface

$$I(z) = I(z+dz) + i\omega C V(z) \Rightarrow -\frac{\partial I}{\partial z} = i\omega C V \qquad (2)$$

where C is the capacitance per unit of length. The equation that describes the potential is finally

$$\frac{\partial^2 V}{\partial z^2} = \frac{i\omega C}{\kappa\pi a^2} V \qquad (3)$$

with boundary conditions of $V(z=0) = V_0$ and $V(z\to\infty) = 0$. Therefore, according to the transmission line model, the potential along the jet is

$$V(z) = V_0 \exp[-(1+i)z/\delta], \text{ where } \qquad \delta = a\sqrt{\frac{2\kappa\pi}{\omega C}} \qquad (4)$$

Strictly speaking, when the jet is finite the boundary condition should be zero current at the tip of the jet (Baret et al., 2005, 2007). However, the penetration length δ is not affected by this choice since it is the characteristic length scale of the transmission line equation (3).

Table 1 Values of the dimensionless relevant parameters involved in this problem.

$\eta_i/\eta_o = 0.01$	$Q_i/Q_o = 0.125$
$Re_o = \rho_o U_o h/\eta_o \simeq 0.01$	$Re_i = \rho_i U_i d_j/\eta_i \simeq 0.7$
$Ca_o = \eta_o U_o/\sigma \simeq 0.5$	$Ca_i = \eta_i U_i/\sigma \simeq 0.02$
$B_{\mathrm{e,cone}} = \varepsilon_o E_{rms}^2 \ell/2\sigma \simeq 0.5$	$B_{\mathrm{e,jet}} = \varepsilon_o E_{rms}^2 d_j/4\sigma \simeq 6$

The capacitance per unit of length C is here obtained numerically using the finite element solver COMSOL and taking into account the dimensions of our system in a cross-section (see Figure 1b). The numerically obtained value for C is 5.1×10^{-11} F/m. The approximation is valid when $\delta \gg a$, i.e. when the characteristic axial length is much greater than the transverse length. For instance, for $\kappa = 10^{-3}$ S/m, $a = 6.5\,\mu$m, $f = 5$ kHz, we get $\delta = 410\,\mu$m and the condition is fulfilled. This value of δ is of the order of the jet lengths observed in experiments. Interestingly, δ is inversely proportional to the square root of frequency, in agreement with the observed trend for jet length with frequency. Figure 7 shows jet length in units of radius a as a function of nondimensional frequency $\Omega = \omega C/\kappa$ for the three conductivities, and the functions δ/a and $2\delta/a$. As can be seen, the jet breaks into drops at a distance from the entrance between δ and 2δ. Since E_{rms}^2 is proportional to $|V|^2 = V_0^2 \exp(-2z/\delta)$, the electrical Bond number decreases from a value $B_{\mathrm{e,jet}} \sim 6$ at the entrance ($z = 0$) to a value $B_{\mathrm{e,jet}} \sim 6\exp(-4) \approx 0.1$ when the jet has already broken into drops (at $z = 2\delta$). Therefore, the jet breaks into drops when the electrical pressure is much smaller than the capillary pressure. It should be noted that from an electrical point of view, the existence of a conducting jet inside the downstream channel is favored because it increases the electrical energy stored in the system, which is at constant potential.

In the model we have performed several approximations that we now justify. We have neglected the convection of charge by the moving jet interface in front of the ohmic current through the jet bulk. The ratio between convection and conduction currents is known as the electric Reynolds number (Melcher and Taylor, 1969). In our case, the convective current at a certain axial location is $I_{conv} = 2\pi a q_s U_i$. Here q_s is the induced surface charge on the jet given approximately by $\varepsilon_o E_n$, with E_n the outer normal electric field. The ohmic current along the jet is $I_{ohm} = \pi a^2 \kappa E_z$ where E_z is the axial electric field. Therefore, the electric Reynolds number is $I_{conv}/I_{ohm} \sim \varepsilon_o \delta U_i 2/\kappa a^2$, where we have taken into account that $E_n/E_z \sim \delta/a$ in our model. For the frequency of the instability (3kHz) and for the smallest conductivity (0.3 mS/m), the ratio between convected and ohmic currents is of the order of 0.05 and we can safely ignore the motion of the jet when computing the fields. We have also neglected the displacement current through the jet bulk in front of the ohmic current. This is valid if $\varepsilon_i \omega/\kappa \ll 1$, which is the case for the signal frequencies we are dealing with, $\varepsilon_i \omega/\kappa \sim 4 \times 10^{-3}$ for $f = 1$ kHz, and $\kappa = 10^{-3}$ S/m. In fact, the model can easily incorporate the displacement current by using a complex conductivity, $\tilde{\kappa} = \kappa + i\varepsilon_i \omega$.

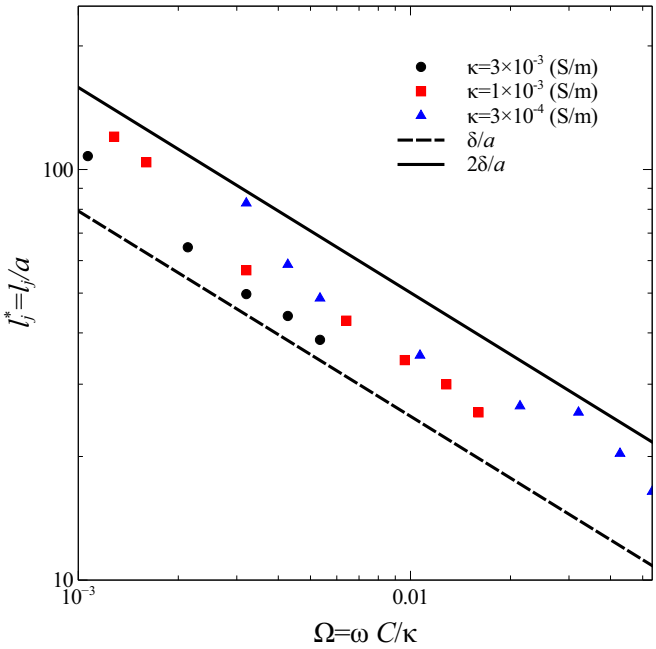

Fig. 7 Dimensionless jet length as a function of nondimensional frequency for different values of the conductivity for $Q_i = 50\,\mu$l/h, $Q_o = 400\,\mu$l/h, $\eta_o = 100$ cP and $V = 1000$ V.

5 Conclusions

In this work we have experimentally studied AC electrified jets in a microfluidic flow-focusing junction. We have shown that in AC electric fields the jet length is a function of both the magnitude of the applied voltage and the electrical parameters such as the frequency of the AC field and the conductivity of the dispersed phase. We have explained this dependency using a simple transmission line model along the liquid jet. The penetration length of the AC electric field along a conducting cylinder determines the length of the liquid jet: the scaling law of the jet length vs the electrical parameters obtained experimentally is fully compatible with our minimal theoretical modeling. In addition, we have observed that the jets become unstable rather abruptly below a certain frequency. In this study, we have shown that AC voltages can elongate dramatically liquid jets, which can be a technological advantage for manufacturing processes where structures with large aspect ratios are required.

Acknowledgements The authors are grateful to the DAAD (German Academic Exchange Service) for the financial support. They would also like to acknowledge financial support

by the ERC (FP7/2007-2013 /ERC Grant agreement 306385–SofI) and from Spanish Government Ministry MEC under Contract No. FIS2011-25161.

References

Abate AR, Romanowsky MB, Agresti JJ, Weitz DA (2009) Valve-based flow focusing for drop formation. Appl Phys Lett 94(2):023,503

Agresti JJ, Antipov E, Abate AR, Ahn K, Rowat AC, Baret JC, Marquez M, Klibanov AM, Griffiths AD, Weitz DA (2010) Ultrahigh-throughput screening in drop-based microfluidics for directed evolution. Proc Natl Acad Sci U S A 107(9):4004–4009

Anna SL, Mayer HC (2006) Microscale tipstreaming in a microfluidic flow focusing device. Phys Fluids 18(12):121,512

Anna SL, Bontoux N, Stone HA (2003) Formation of dispersions using Flow Focusing in microchannels. Appl Phys Lett 82:364–366

Ashcroft RG, Lopez PA (2000) Commercial high speed machines open new opportunities in high throughput flow cytometry (htfc). J Immunol Methods 243(1-2):13–24

Baret JC, Decré M, Herminghaus S, Seemann R (2005) Electroactuation of fluid using topographical wetting transitions. Langmuir 21(26):12,218–12,221

Baret JC, Decr MMJ, Herminghaus S, Seemann R (2007) Transport dynamics in open microfluidic grooves. Langmuir 23(9):5200–5204

Castro-Hernández E, Campo-Cortés F, Gordillo JM (2012) Slender-body theory for the generation of micrometre-sized emulsions through tip streaming. J Fluid Mech 698:423–445

Cordero ML, Gallaire F, Baroud CN (2011) Quantitative analysis of the dripping and jetting regimes in co-flowing capillary jets. Phys Fluids 23(9):094,111

Cramer C, Fischer P, Windhab EJ (2004) Drop formation in a co-flowing ambient fluid. Chem Eng Sci 59(15):3045–3058

Cubaud T, Mason TG (2008) Capillary threads and viscous droplets in square microchannels. Phys Fluids 20:053,302

Dangla R, Kayi SC, Baroud CN (2013) Droplet microfluidics driven by gradients of confinement. Proc Natl Acad Sci U S A 110(3):853–858

Debs BE, Utharala R, Balyasnikova IV, Griffiths AD, Merten CA (2012) Functional single-cell hybridoma screening using droplet-based microfluidics. Proc Natl Acad Sci U S A 109(29):11,570–11,575

Eggers J, Villermaux E (2008) Physics of liquid jets. Rep Prog Phys 71:036,601

Gañán-Calvo AM (1998) Generation of steady liquid microthreads and micron-sized monodisperse sprays in gas streams. Phys Rev Lett 80:285–288

Gañán-Calvo AM (2002) Capillary jets and micro/nanometric particles production device uses electrohydrodynamic force, fluid-dynamic force and specific geometry to produce micro or nano capsules which are disintegrated to form drops of micro or nano size. Pats no ES2199048 (A1) & (B1),

Gañán-Calvo AM (2007) Electro-flow focusing: The high-conductivity low-viscosity limit. Phys Rev Lett 98:134,503

Gañán-Calvo AM (2008) Unconditional jetting. Phys Rev E 78:026,304

Gañán-Calvo AM, López-Herrera JM (2002) Device for the production of capillary jets and micro- and nanometric particles. Pats no EP1479446 (A1), AT392262 (T), US2005116070 (A1), US7341211 (B2) & others

Gañán-Calvo AM, López-Herrera JM, Riesco-Chueca P (2006) The combination of electrospray and flow focusing. J Fluid Mech 566:421–445

Gañán-Calvo AM, González-Prieto R, Riesco-Chueca P, Herrada MA, Flores-Mosquera M (2007) Focusing capillary jets close to the continuum limit. Nature Phys 3:737–742

Gopalan B, Katz J (2010) Turbulent shearing of crude oil mixed with dispersants generates long microthreads and microdroplets. Phys Rev Lett 104:054,501

Guillot P, Colin A, Utada AS, Ajdari A (2007) Stability of a jet in confined pressure-driven biphasic flows at low Reynolds numbers. Phys Rev Lett 99:104,502

Guillot P, Colin A, Ajdari A (2008) Stability of a jet in confined pressure-driven biphasic flows at low Reynolds number in various geometries. Phys Rev E 78:016,307

Guo MT, Rotem A, Heyman JA, Weitz DA (2012) Droplet microfluidics for high-throughput biological assays. Lab Chip 12:2146–2155

Herrada MA, Gañán-Calvo AM, Guillot P (2008) Spatiotemporal instability of a confined capillary jet. Phys Rev E 78:046,312

Huebner A, Sharma S, Srisa-Art M, Hollfelder F, Edel JB, et al. (2008) Microdroplets: a sea of applications? Lab Chip 8(8):1244–1254

Kim H, Luo D, Link D, Weitz DA, Marquez M, Cheng Z (2007) Controlled production of emulsion drops using an electric field in a flow-focusing microfluidic device. Appl Phys Lett 91(13):133,106

Malloggi F, Gu H, Banpurkar AG, Vanapalli SA, Mugele F (2008) Electrowetting –a versatile tool for controlling microdrop generation. Eur Phys J E Soft Matter 26(1-2):91–96

Melcher J, Taylor G (1969) Electrohydrodynamics: a review of the role of interfacial shear stresses. Annu Rev Fluid Mech 1(1):111–146

Miller OJ, Bernath K, Agresti JJ, Amitai G, Kelly BT, Mastrobattista E, Taly V, Magdassi S, Tawfik DS, Griffiths AD (2006) Directed evolution by in vitro compartmentalization. Nat Methods 3(7):561–570

Miller OJ, Harrak AE, Mangeat T, Baret JC, Frenz L, Debs BE, Mayot E, Samuels ML, Rooney EK, Dieu P, Galvan M, Link DR, Griffiths AD (2012) High-resolution dose-response screening using droplet-based microfluidics. Proc Natl Acad Sci U S A 109(2):378–383

Nguyen NT, Ng KM, Huang X (2006) Manipulation of ferrofluid droplets using planar coils. Appl Phys Lett 89(5):052,509

Pekin D, Skhiri Y, Baret JC, Corre DL, Mazutis L, Salem CB, Millot F, Harrak AE, Hutchison JB, Larson JW, Link DR, Laurent-Puig P, Griffiths AD, Taly V (2011) Quantitative and sensitive detection of rare mutations using droplet-based microfluidics. Lab Chip 11:2156–2166

Ramo S, Whinnery JR, Van Duzer T (2008) Fields and waves in communication electronics. John Wiley & Sons

Schmid L, Franke T (2013) Saw-controlled drop size for flow focusing. Lab Chip 13(9):1691–1694

Sciambi A, Abate AR (2014) Accurate microfluidic sorting of droplets at 30 khz. Lab Chip 15(1):47–51

Seemann R, Brinkmann M, Pfohl T, Herminghaus S (2012) Droplet-based microfluidics. Reports on Progress in Physics 75:016,601

Siegel AC, Shevkoplyas SS, Weibel DB, Bruzewicz DA, Martinez AW, Whitesides GM (2006) Cofabrication of electromagnets and microfluidic systems in poly(dimethylsiloxane). Angew Chem 118:7031–7036

Tan SH, Nguyen NT (2011) Generation and manipulation of monodispersed ferrofluid emulsions: The effect of a uniform magnetic field in flow-focusing and t-junction configurations. Phys Rev E 84(3):036,317

Tan SH, Murshed SS, Nguyen NT, Wong TN, Yobas L (2008) Thermally controlled droplet formation in flow focusing geometry: formation regimes and effect of nanoparticle suspension. J Phys D: Appl Phys 41(16):165,501

Tan SH, Maes F, Semin B, Vrignon J, Baret JC (2014a) The microfluidic jukebox. Scientific reports 4:4787

Tan SH, Semin B, Baret JC (2014b) Microfluidic flow-focusing in ac electric fields. Lab Chip 14(6):1099–1106

Thorsen T, Roberts RW, Arnold FH, Quake SR (2001) Dynamic pattern formation in a vesicle-generating microfluidic device. Phys Rev Lett 86(18):4163

Utada AS, Fernández-Nieves A, Gordillo JM, Weitz D (2008) Absolute instability of a liquid jet in a coflowing stream. Phys Rev Lett 100:014,502